

# INFLUENCE OF ELECTRON BEAM WELDING TECHNOLOGY ON THE WIDTH OF THE SOFTENING ZONE OF ALUMINIUM 2219 ALLOY

**V.V. Skryabinskyi, V.M. Nesterenkov, M.O. Rusnyk, V.I. Zagornikov,  
O.I. Goncharenko, I.M. Klochkov**

E.O. Paton Electric Welding Institute of the NASU  
11 Kazymyr Malevych Str., 03150, Kyiv, Ukraine

## ABSTRACT

During electron beam welding (EBW) of 2219 alloy, the strength characteristics of joints can decrease by up to 50 % in relation to the base metal. In order to ensure the uniform strength of the structure, the locations of the welds are chosen in thickened areas. At the same time, the width of the thickened area should be greater than the width of the softening zone of the welded joint. This zone includes the cast zone and the heat-affected zone (HAZ), in which the strength of the base metal decreased. The influence of welding speed and the use of process pads on the width of the cast zone and the HAZ, i.e. on the width of the softening zone during EBW of 2219 alloy plates were studied. It was found that an increase in the welding speed from 10 to 20 mm/s reduced the width of the softening zone approximately by a half. The use of the process pad allows reducing the width of the softening zone by approximately 20 %. In this case, the weld underfill is formed in the body of the pad and after its removal the welded butt does not require further mechanical treatment. It was established by calculation and experimental methods that the process pad cuts off the peripheral part of the electron beam, which is about 5 % of its full power. In practice, the influence of this peripheral part leads to undesirable expansion of the weld on the side of the beam entrance and to additional heating of the base metal and, as a result, to an increase in the size of the softening zone.

**KEYWORDS:** electron beam welding, aluminium alloy, heat affected zone, softening zone, process pad

## INTRODUCTION

The high-strength aluminium 2219 alloy of the Al–6Cu alloying system is a heat-treatable alloy. The high mechanical properties of such alloys are achieved as a result of heat treatment, at which secondary strengthening phases are precipitated. During welding of such alloys, these phases dissolve in the heat-affected zone (HAZ), which causes a decrease in the strength characteristics of the metal. The beginning of the dissolution process is featured not only by the maximum heating temperature, but also by the duration of staying in the corresponding temperature range [1].

The electron beam welding (EBW) process is characterized by a very short thermal cycle period with high cooling rates and a small volume of molten metal. This leads to a significant reduction in the size of the HAZ [2, 3]. Despite this, the strength of welded joints remains quite low. For example, even at short-term heating typical for EBW, the strength factor of Al–6Cu alloy joints is 70–75 % [4] and sometimes less than 50 % [5]. In order to ensure a uniform structural strength, weld locations are chosen in thickened areas. Moreover, the width of the thickened area should be greater than the width of the softening zone of the welded joint. On the other hand, an excessive increase in the width of such areas leads to an undesirable increase in the overall

weight of the structure. The softening zone of the joint includes the cast zone and the HAZ, where the strength of the base metal decreased. In order to reduce the weight of structures, it is necessary to choose the EBW conditions, which ensure the production of welds with a minimum width of the cast zone and HAZ. Electron beam welding allows producing such joints. High energy concentration allows welding metals at high speed with a small weld pool volume.

The EBW of aluminium alloys has its own peculiarities. In many cases, the penetration has a wedge shape [5–8]. This is predetermined by the fact that the distribution of the electron beam power density along its cross-section is close to the normal distribution law [9]. The central part of the beam with the highest energy concentration melts the metal and ensures its welding. The peripheral parts of the beam hitting the edges of the metal being welded melt them, thereby increasing the width of the weld on the side of the beam entrance. In addition, the edges of this peripheral part of the beam, which no longer have enough power to melt the metal, directly heat the edges to be welded, increasing the HAZ width.

Typical cross-sections of joints of aluminium Al–6Cu system alloys welded by electron beam are shown in Figure 1. In all cases, the welds are wider at the beam entrance than at the root part. Also, a slight

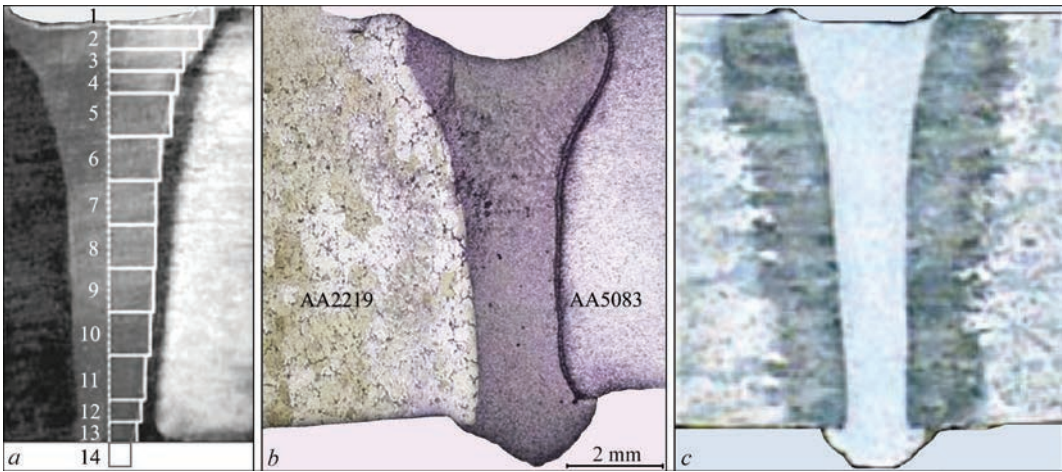


**Figure 1.** Typical cross-sections of welds at EBW of Al-6Cu alloy: *a* — [6]; *b* — [7]; *c* — [8]

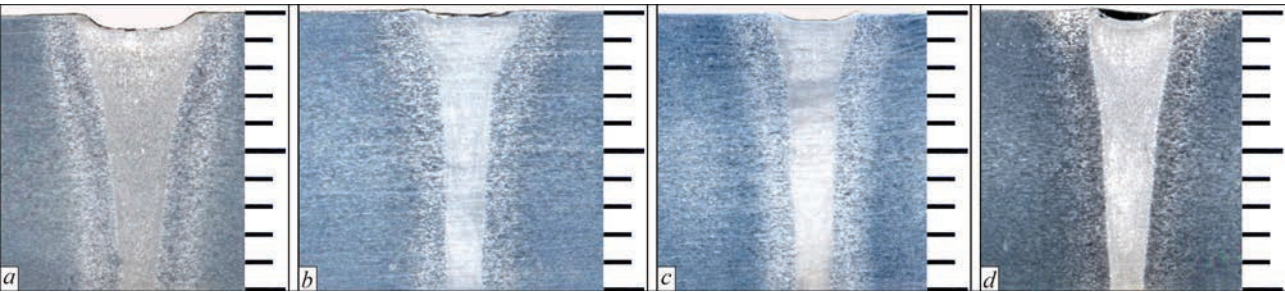


**Figure 2.** Cross-sections of welds at EBW of 2219 alloy at welding speed: *a* — 10; *b* — 15; *c* — 20; *d* — 25 mm/s

underfill of the weld metal is seen on the beam entrance side.

**THE AIM**

of this work is to determine the technology for EBW of 2219 alloy plates, which ensures the production of joints with a minimum width of the softening zone.

**DESCRIPTION OF THE MAIN MATERIAL**

Welding was carried out in an electron beam welding installation UL-209M with an ELA 60/60 power source. The hardness of the weld metal and HAZ were measured by the Vickers method, using the M-400 hardness tester by LECO. The load was 1N (100 g), the time of load application was 10 s. The plates of aluminium 2219 T8 alloy with a thickness of 10 mm were welded. The parameters of the welding conditions (Table 1) were selected in such a way as to provide complete penetration of the butt in one pass with the formation of reinforcement and reverse weld bead.

**Table 1.** EBW conditions for 2219 alloy plates

Metal thickness, mm	10	10	10	10	12.2*
Accelerating voltage, kV	60	60	60	60	60
Welding speed, mm/s	10	15	20	25	20
Beam current, mA	55	70	85	95	95
* – 10 mm + 2.2 mm thick pad.					

In all experiments, a circular beam scanning trajectory was used at an amplitude of 1 mm and a scan frequency of 580 Hz with focusing on the surface of the plates to be welded. I.e., the relative distribution of the electron beam power density was maintained constant. Cross-sections of welds at EBW of 2219 alloy at welding speeds of 10, 15, 20 and 25 mm/s are shown in Figure 2.

The widest welds (see Table 2) were produced by welding at a speed of 10 mm/s. The cast zone is wedge-shaped, its width is 5.5 mm on the beam entrance side and 1.6 mm on the beam exit side. When the speed was increased to 15 mm/s, the width of the cast zone decreased to 3.6 and 1.4 mm, respectively. The further increase in the welding speed did not significantly affect the width of the cast zone.

**Table 2.** Width of the weld cast zone depending on the welding speed

Welding speed, mm/s	10	15	20	25*	20 (welding with the pad)
Width of the cast zone on the beam entrance side, mm	5.5	3.6	3.6	3.6	1.6
Width of the cast zone on the beam exit side, mm	1.6	1.4	1.4	1.3	1.4
*Weld with defects.					



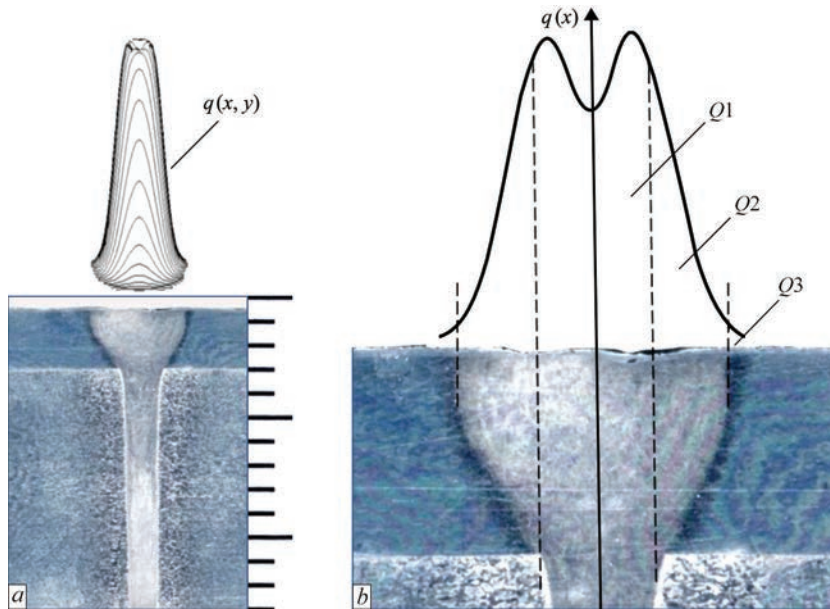


**Figure 3.** Distribution of beam power density (*a* —  $q(x, y)$  and *b* —  $q(x)$ ) and cross-section of 2219 alloy weld produced using a pad made of the same alloy

The expansion of the cast zone from the beam entrance is caused by the presence of a peripheral part of the beam with a relatively low power density. In order to exclude the influence of the peripheral part of the beam on the penetration shape, a welding technique with the pad of the same material was used. Such pads during welding with complete penetration not only shield the peripheral parts of the beam, but also serve as a filler material. The underfill in the weld is formed in the body of the pad. After welding, the pad is removed by mechanical treatment.

It was noted that at speeds of 10, 15 and 20 mm/s, the welding process is carried out with stable joint formation both from the face and root parts of the weld. When the welding speed is increased to 25 mm/s, the stability of the weld formation is violated. Defects such as poor penetration and slight metal leakage periodically appear in the root part of the weld. Therefore, welding with the process pad was carried out at the maximum speed that ensures a stable process, i.e. at 20 mm/s.

In Figure 3, the cross-section of the weld produced with the pad was schematically combined with the volumetric diagram of the beam power density distribution (Figure 3, *a*) and the cross-section of this diagram (Figure 3, *b*). It is seen from the Figure that the cast zone is narrow and has an almost rectangular shape. The width of the cast weld zone under the pad is 1.6 mm and 1.4 mm on the beam exit side, with a maximum pad partial melting width of 5 mm. The central part of the electron beam with the highest energy concentration and power  $Q1$  ensures complete penetration of the metal to be welded and the process pad. The side peripheral parts of the beam with a low

energy concentration are shielded by the process pad. At the same time, they partially melt (power  $Q2$ ) and heat (power  $Q3$ ) the pad.

It is interesting to determine how much of the electron beam power is shielded by the process pad. It can be calculated or measured experimentally. The previously developed algorithm for calculating the distribution of electron beam power density [10] allows calculating the ratio of beam powers in any selected treatment areas. For the calculations, a software for designing electron beam scans was used [11]. Figure 4 shows the distribution of the power density of an electron beam with an effective diameter of 0.5 mm for a scan in the form of a circle with a diameter of

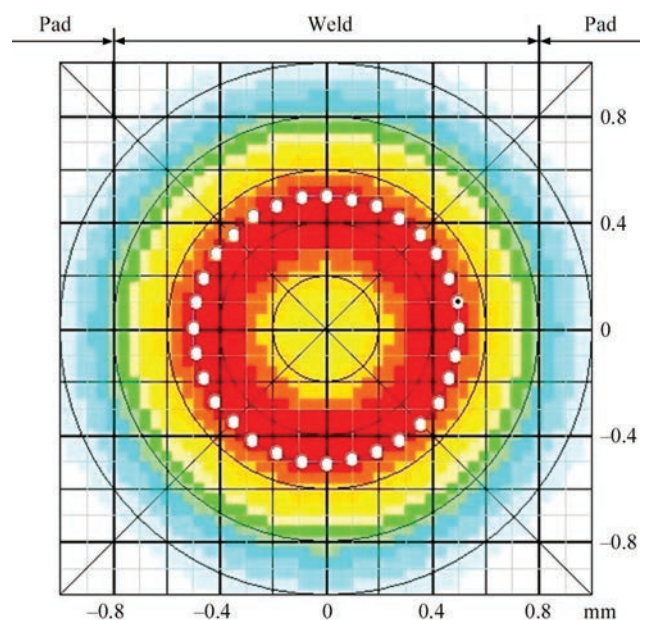


**Figure 4.** Color image of the beam power density distribution  $q(x, y)$  displayed on the computer screen



**Figure 5.** Experimental measurement of the beam power shielded by the process pad

1 mm. The colours represent the beam power intensity from minimum (blue) to maximum (red).

A part of the electron beam power that falls on the weld area with complete penetration ( $Q1$ , %) can be calculated by the formula:

$$Q1(\%) = \frac{100 \iint_{WMe} q(x, y) dx dy}{\iint_{Me} q(x, y) dx dy},$$

where  $q(x, y)$  is the distribution of beam power density;  $WMe$  is the area of beam effect that falls on the weld metal;  $Me$  is the entire area of electron beam treatment. Similarly, it is possible to calculate a part of the beam power that is consumed for partial melting ( $Q2$ , %) and heating ( $Q3$ , %) of the pad metal on both sides of the weld.

Calculations have shown that in our case, about 95 % of the electron beam power is directed at the weld, and about 2.5 % of the beam power on each side is directed to heating and melting the parts of the pad adjacent to the weld, respectively. The experimental measuring of the electron beam power directed at a certain area to be treated is possible by placing a refractory metal target in this area and measuring the amount of current passing through the target. The beam power shielded by the pad was determined as follows. Molybdenum plates with a thickness of 6 mm were fixed in the assembly and welding device with a gap of 1.6 mm between them. The width of the gap was equal to the width of the weld under the process pad. The plates were placed on the ceramic insulators and fixed with clamps through the ceramic insulators, as shown in Figure 5.

These insulators electrically isolated the plates from the welding chamber, i.e. from “ground”. The electric wires connected to the molybdenum plates were removed from the vacuum chamber and connected to ‘ground’ through voltage dividers. Electric currents passing through the plates were measured by voltmeters connected to voltage dividers. A basic secondary electronic video surveillance system of the RASTR6 type was used to direct the beam to the centre of the gap between the plates. After that, the welding process was simulated at the conditions used for welding the 2219 alloy plates with the pad (i.e., at a beam current of 95 mA, see Table 1). When the beam was precisely aimed at the centre of the gap, the readings of voltmeters during the experiment coincided. During the measurement, the currents of the plates fluctuated within 2.5–3.5 mA. Thus, approximately 5 to 7 % of the total beam power fell on both plates. The total width of the softening zone of the welded

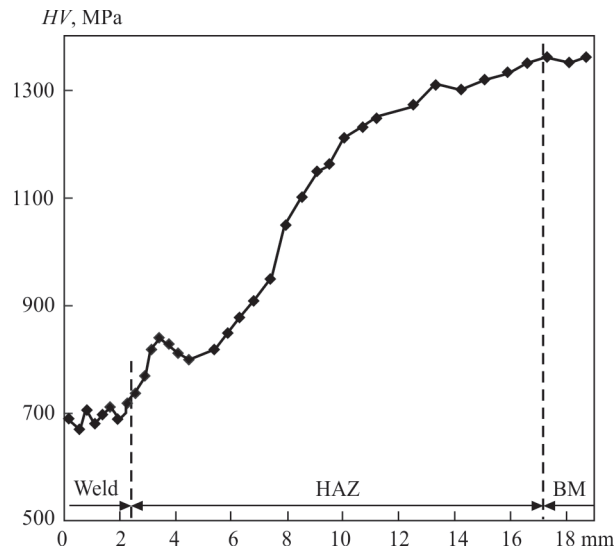


**Figure 6.** Distribution of hardness in the cross-section of joints in 2219 alloy plates welded at a speed of 10 mm/s

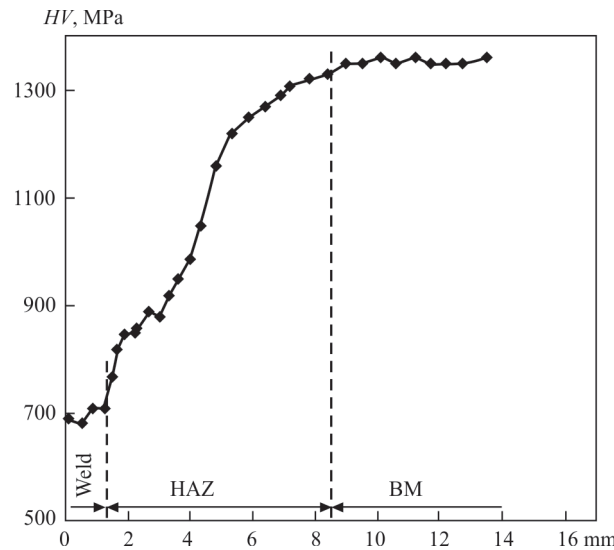


**Figure 7.** Distribution of hardness in the cross-section of joints in 2219 alloy plates welded at a speed of 20 mm/s

**Table 3.** Width of the HAZ and softening zone depending on the welding speed and during welding with the process pad

Welding speed, mm/s	10	15	20	25*	20 (welding with the pad)
Maximum width of the cast zone, mm	5.5	3.6	3.6	3.6	1.6
Width of HAZ from the fusion line to the base metal, mm	15	10	7	6	6
Width of the softening zone, mm	35.5	23.6	17.6	15.6	13.6

\*Weld with forming defects.

joint is equal to the width of the cast zone plus the width of the HAZ on both sides of it. The width of the HAZ was determined by measuring the hardness of the cross-sections of the welded joints at distances of 1.5 mm from the plate surface on the beam entrance side. The measurement step was 0.3–0.5 mm. The measurements started from the centre of the weld and ended in 3–5 mm after reaching the base metal. The distribution of hardness in the cross-sections of the joints of 2219 alloy plates welded at speeds of 10 and 20 mm/s is shown in Figures 6 and 7.

The hardness of the weld metal is 670–710 MPa, while the hardness of the base metal is 1350–1360 MPa. When the welding speed was increased from 10 to 20 mm/s, the HAZ width decreased from 15 to 7 mm. It is seen that the hardness of the metal at a distance of 1 mm from the fusion line is by 30–40 MPa higher than the hardness measured at a distance of 2–3 mm. This is predetermined by the partial hardening of the metal in the immediate vicinity of the weld after it was heated to the quenching temperature and then rapidly cooled. The cross-sectional hardness distribution of the joints of 2219 alloy plates welded with the process pad is shown in Figure 8.

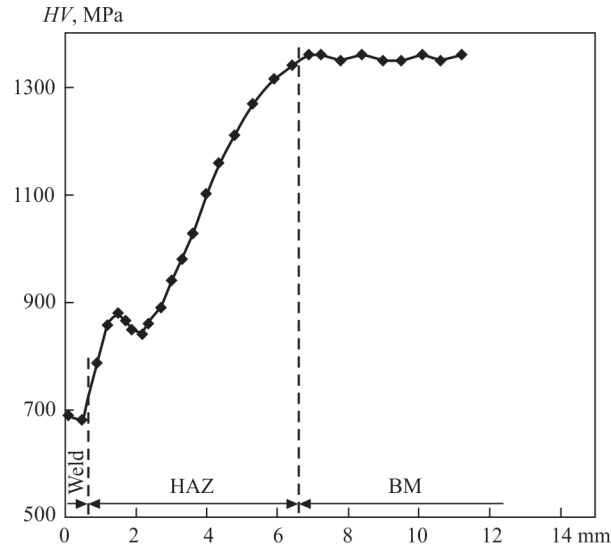
Table 3 shows the dependence of the HAZ width and softening zone on the welding speed.

Table shows that an increase in the welding speed from 10 to 20 mm/s reduces the width of the softening zone by almost half (from 35.5 to 17.6 mm). The further increase in the welding speed is inappropriate because it will cause violation of the joint formation stability and appearance of defects.

The use of the process pad during EBW of 10 mm thick aluminium 2219 alloy plates allows reducing the width of the softening zone from 17.6 to 13.6 mm (i.e. by about 20 %) on the beam entrance side and producing a narrow weld with practically parallel side walls.

CONCLUSIONS

It has been found that during EBW of 2219 aluminium alloy plates with a thickness of 10 mm, an increase in



**Figure 8.** Distribution of hardness in the cross-section of joints in 2219 alloy plates welded with the technological pad at a speed of 20 mm/s

the welding speed from 10 to 20 mm/s reduces the width of the softening zone approximately by a half.

The use of the process pad when welding at a speed of 20 mm/s allows for an additional reduction in the width of the softening zone by approximately 20 % and produces a narrow weld with almost parallel side walls. In this case, the weld underfill is formed in the body of the pad; after its removal, the welded butt does not require further mechanical treatment.

An algorithm for calculating the ratio of beam powers in selected areas of the treated surface was proposed. It has been found by calculations and experiments that the technological pad cuts off the peripheral part of the electron beam, which is about 5–7 % of its total power. In practice, the influence of this peripheral part leads to undesirable expansion of the weld on the beam entrance side and to additional heating of the base metal and, as a result, to an increase in the sizes of the softening zone.

REFERENCES

1. Lozovskaya A.V., Chajka A.A., Bondarev A.A., Poklyatsky A.G., Bondarev Andr.A. (2001) Softening of high-strength aluminium alloys in different fusion welding processes. *The Paton Welding J.*, **3**, 13–17. <https://patonpublishinghouse.com/tpwj/pdf/2001/tpwj200103all.pdf>

2. Fatih Hayat (2022) Electron beam welding of 7075 aluminium alloy: Microstructure and fracture properties. *Engineering Sci. and Technol. an Inter. J.*, **34**, 101093. DOI: <https://doi.org/10.1016/j.jestch.2022.101093>

3. Meng, Qing-guo, Fang, Hong-yuan, Xu, Wen-li, Ji, Shu-de (2006) Microstructure and mechanical properties of 2219 Al-alloy heat-affected zone with twin wire welding. *Transact. of the China Welding Institution*, **3**, 9–12. DOI: <https://hjxb.hwi.com.cn/hjxb/en/article/id/20060303>

4. Nazarenko, O.K., Kajdalov, A.A., Kovbasenko, S.N. et al. (1987) *Electron beam welding*. Ed. by B.E. Paton. Kyiv, Naukova Dumka.



5. Ghulam Hussain, Tauheed Shehbaz, Mohammed Alkahtani, Usman Abdul Khaliq, Hongyu Wei (2024) Nanomechanical, mechanical and microstructural characterization of electron beam welded Al2219-T6 tempered aerospace grade alloy: A comprehensive study. *Heliyon*, 10(1), e23835. DOI: <https://doi.org/10.1016/j.heliyon.2023.e23835>
6. Skalsky, V.R., Botvina, L.R., Lyasota, I.N. (2012) Peculiarities of structure and mechanical heterogeneity in EB-welded joints of 1201-T alloy. *The Paton Welding J.*, 7, 15–18. <https://patonpublishinghouse.com/tpwj/pdf/2012/pdfarticles/07/5.pdf>
7. Mastanaiah P., Abhay Sharma, Madhusudhan Reddy G. (2018) Process parameters-weld bead geometry interactions and their influence on mechanical properties: A case of dissimilar aluminium alloy electron beam welds. *Defence Technology*, 14, 137–150. DOI: <https://doi.org/10.1016/j.dt.2018.01.003>
8. Rusynyk, M.O., Nesterenkov, V.M., Sahul, M., Klochkov, I.M. (2023) Influence of electron beam focusing current on geometry and microstructure of welded joints of aluminium 2219 alloy. *The Paton Welding J.*, 7, 31–36. DOI: <https://doi.org/10.37434/tpwj2023.07.04>
9. Rykalin, N.N., Zuyev, I.V., Uglov, A.A. (1978) Basis of electron-beam material processing. Moscow, Mashinostroenie [in Russian].
10. Skryabinskyi, V.V. (1994) *Development of technology of electron beam welding of high-strength aluminium alloys 1570 and 1460 with control of density distribution of beam power*: Syn. of Thesis for Cand. of Techn. Sci. Degree. Kyiv, PWI [in Ukrainian].
11. Skryabinskyi, V.V., Nesterenkov V.M., Rusynyk, M.O. (2020) Electron beam welding with programming of beam power density distribution. *The Paton Welding J.*, 1, 49–53. DOI: <https://doi.org/10.37434/tpwj2020.01.07>

## ORCID

V.V. Skryabinskyi: 0000-0003-4470-3421,  
V.M. Nesterenkov: 0000-0002-7973-1986,  
M.O. Rusynyk: 0000-0002-7591-7169,  
V.I. Zagornikov: 0000-0003-0456-173X,  
O.I. Goncharenko: 0009-0007-8492-7119,  
I.M. Klochkov: 0000-0001-6490-8905

## CONFLICT OF INTEREST

The Authors declare no conflict of interest

## CORRESPONDING AUTHOR

V.V. Skryabinskyi  
E.O. Paton Electric Welding Institute of the NASU  
11 Kazymyr Malevych Str., 03150, Kyiv, Ukraine.  
E-mail: [skryabinski.vv.555@gmail.com](mailto:skryabinski.vv.555@gmail.com)

## SUGGESTED CITATION

V.V. Skryabinskyi, V.M. Nesterenkov, M.O. Rusynyk, V.I. Zagornikov, O.I. Goncharenko, I.M. Klochkov (2025) Influence of electron beam welding technology on the width of the softening zone of aluminium 2219 alloy. *The Paton Welding J.*, 6, 19–24.  
DOI: <https://doi.org/10.37434/tpwj2025.06.03>


## JOURNAL HOME PAGE

<https://patonpublishinghouse.com/eng/journals/tpwj>

Received: 04.03.2025

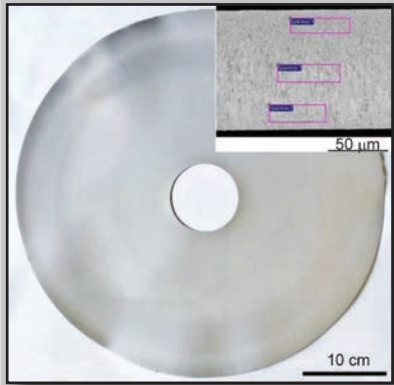
Received in revised form: 06.05.2025

Accepted: 25.06.2025

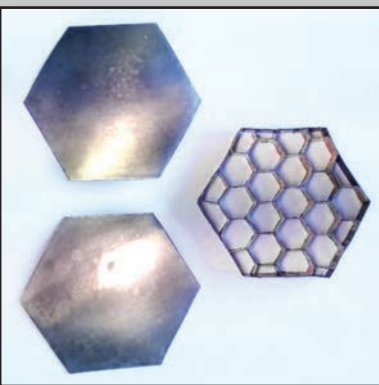


**Developed at PWI**

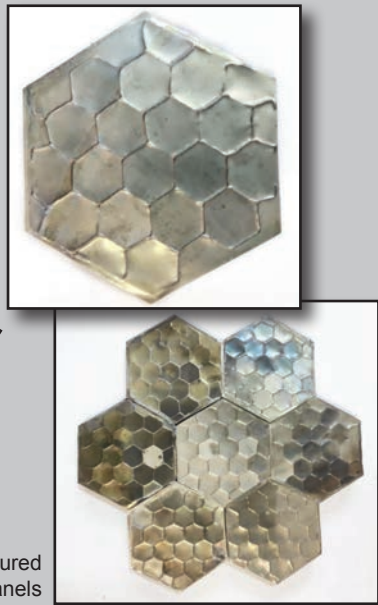
**Fabricating lightweight thermal protection honeycomb sandwich panels based on thin-sheet heat-resistant alloys produced by vacuum deposition**



Appearance and microstructure (inset) of the cross-section CoCrFeNiSi<sub>0.2</sub> high-entropy alloys foil



General view of the the manufactured elements of the three-layer panel (lower and upper cover sheets, honeycomb core)



General view of the manufactured three-layer honeycomb panels

For more information, please follow the link <https://doi.org/10.37434/tpwj2023.08.03>